Chasing the wave in a reverberation chamber

DOI:
10.1109/EMCEurope.2018.8485050

Document status and date:
Published: 05/10/2018

Document Version:
Accepted manuscript including changes made at the peer-review stage

Chasing the Wave in a Reverberation Chamber

L.A. Bronckers, A. Roc'h and A.B. Smolders

Eindhoven University of Technology, Department of Electrical Engineering, Eindhoven, The Netherlands.
Email: l.a.bronckers@tue.nl

***Abstract*—The power-delay profile is a critical characteristic of a reverberation chamber. In this paper the power-delay profile is used for the first time to study in high detail how a wave interacts with its environment in a reverberation chamber. This is done by tracking the wave, starting from its creation at the antenna reference plane with the antenna in multiple positions. Starting at the antenna port, three regimes are recognized: very-early-time, early-time and late-time. In the very-early-time the response is dictated by the antenna's behavior and placement affects only the duration of this regime. In the early-time period the wave starts interacting with the environment. Antenna positioning makes a clear difference during this period, and the moving-wall stirrer can easily be distinguished from non-moving parts. During late-time the expected exponential decay is observed. The transition point from early to late behavior is dependent on antenna placement in the room that was used. After chasing the wave traveling at light speed for a kilometer, it is finally caught when the chamber losses cause the power delay profile to decay into noise floor.**

I. Introduction

Next to their EMC applications, reverberation chambers (RC's) are often used for wireless communication, such as the testing of wireless communication (MIMO) devices under a realistic channel model [1]–[8]. Among other applications these methods often make use of loading the chamber, thereby changing the power-delay profile (PDP) of the room to simulate real-life scattering environments. Since this relies on the RC's stochastic behavior, it assumes that randomness (or stochastic field uniformity) is reached within the chamber's working volume. Before this is reached, the energy in the chamber has to build-up [3]. This paper describe experimentally, and for the first time, some very interesting effects occurring during this process. Three stages in time can be distinguished in an RC. These are studied by following the wave as it travels, showing the distinct behaviors and properties of each period. This investigation also allows testing of the antenna positioning (in)dependence of the PDP in each of the three stages in time. While the PDP has been studied in various fashions [1], [3], [5], [9], [10], this is, to the best of the authors' knowledge, the first paper in which three time-regimes are recognized, and where interaction between the antennas and the room is studied in this manner.

This paper is set up according to the three phases, and travels along with the wave. Before the waves are launched, the experiment is set up in Section II. Next, the waves are released from the SMA connector and encounter the antenna followed by air, which is observed in the very-early-time behavior in Secion III. Inevitably in an RC, the waves will then run into a wall and separate their ways. This period is described in Section IV, which treats the early-time behavior. Next, the waves become fully separated and obtain their desired statistical behavior in the late-time behavior, Section V. Finally the waves decay to the noise floor, leading to the Conclusion in Section VI.

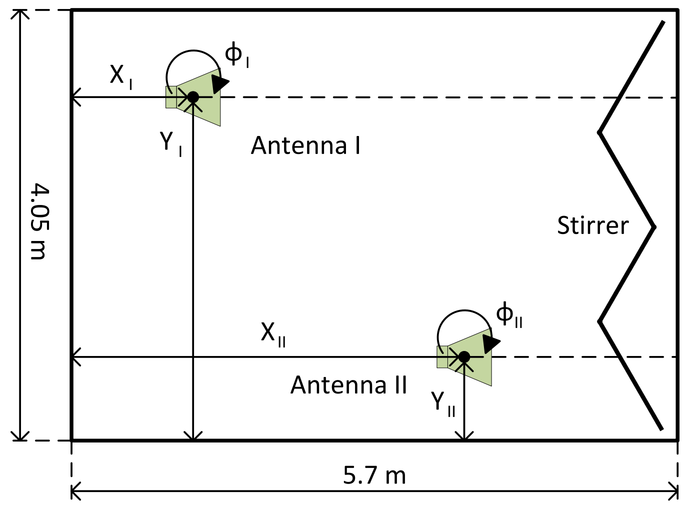

Fig. 1. Top view of the antenna placement in the reverberation chamber.

II. The experiment

To obtain the time-domain data, measurements are performed in frequency domain using a VNA in the maximum range allowed by the antennas (double ridged horns): 0.75-18 GHz. Frequency samples are taken equidistantly spaced over the entire range with 10.000 points/GHz. The VNA is calibrated up to the antenna connectors, defining time $t = 0$ and distance $d = 0$ at that plane. The antennas are positioned in the reverberation chamber at Eindhoven University of Technology (TU/e), which is a 4.05 x 5.7 x 3.15 m^3 room that uses a folding wall as stirring mechanism [11]. The center hinge can travel over approximately 1.0 m back and forth (40 cm from the wall in its backmost position), and $N = 100$ linear stirrer positions are used with this mechanism, i.e. a 1 cm step. A top view of the room and antenna positions is given in Fig. 1. Three cases are studied, which are indicated by Case A, Case B and Case C. Between Case A and Case B, both antennas are moved; between Case B and Case C only antenna II is rotated. The positions of the antennas are given

TABLE I
APPROXIMATE LOCATIONS OF ANTENNAS

	X_{I} [m]	Y_{I} [m]	Z_{I} [m]	ϕ_{I} [Degrees]	θ_{I} [Degrees]	R_{I} [m]	X_{II} [m]	Y_{II} [m]	Z_{II} [m]	ϕ_{II} [Degrees]	θ_{II} [Degrees]	R_{II} [m]	$D_{\text{I-II}}$ [m]
Case A	1.1	2.6	0.9	80	25	1.7	3.0	1.1	0.7	200	25	1.6	2.4
Case B	1.5	2.7	0.9	45	25	3.3	1.9	1.2	0.7	200	25	2.9	1.6
Case C	1.5	2.7	0.9	45	25	3.3	1.9	1.2	0.7	300	25	1.5	1.6

in Table I, and antenna I is connected to port 1 of the VNA while antenna II is connected to port 2 of the VNA (so S_{11} corresponds to antenna I while S_{22} corresponds to antenna II). The height above the floor of each antenna is indicated by the Z-component, while their elevation angle (w.r.t. horizontal) is indicated by θ. In addition, the distance from the antenna to the nearest reflecting surface at boresight is given by R_{I} and R_{II} for antennas I and II, respectively. For Case A and Case B R_{II} is given with respect to the stirrer front plane with the stirrer in its frontmost position. The distance between the antenna centers is indicated as $D_{\text{I-II}}$. Please note that all dimensions given are approximate. For convenience, the approximate locations and orientations are also illustrated in the top view shown in Fig. 2.

After the measurement, the PDP can be calculated using $\text{PDP}(t) = \langle|\text{ifft}[S_{ij_n}(f)]|^2\rangle$ [1], [3], [9], [10], where $\langle\cdot\rangle$ denotes the ensemble average, ifft$[\cdot]$ signifies the inverse Fourier transform, and S_{ij_n} is the ij^{th} S-parameter in stirrer position n. Before taking the inverse Fourier transform, a Hamming window is applied to the data to reduce ringing. Then, the inverse Fourier transform is taken on the complex S-parameter data for each S-parameter and stirrer position, before taking the ensemble average over n of their magnitudes squared to obtain the PDP. For reflection parameters the time scale is multiplied by half the speed of light to obtain distance; for transmission parameters the time scale is multiplied by the speed of light. This results in a PDP as a function of distance, in which the position of reflections on the path traveled can be observed. This PDP is referred to as 'the wave' throughout this paper. The curve order in the figures is chosen per figure to display the results most clearly.

III. VERY-EARLY-TIME

In the very-early-time behavior, the wave has not yet interacted with its environment. It is best observed on a logarithmic scale. S_{11} and S_{22} are shown in Fig. 4 and 5, respectively. Since the antennas differ, the very-early-time behavior of the S_{11}'s differs from that of the S_{22}'s. Nevertheless, the behavior does not change between Cases A, B and C, while the positions are significantly changed. The small differences that can be observed are most likely due to measurement errors due to e.g. noise, drift, and cable movement.

Considering antenna I, the estimated distance to a reflecting surface at boresight is 1.7 m in Case A and 3.3 m in Case B and Case C, as indicated in Table I. In Fig. 4 it can be seen that in Case A the first distinct peak occurs at 1.7 m, and slightly more spread out for Case B and C at 3.4 m. For antenna II in

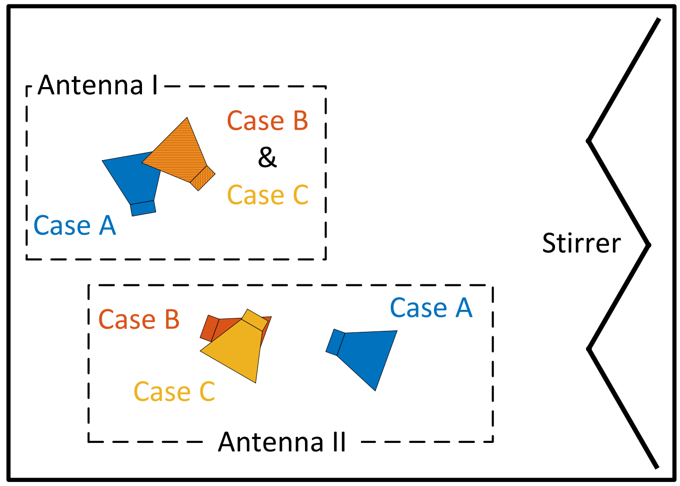

Fig. 2. Top view of the approximate antenna locations for Case A, Case B and Case C in the reverberation chamber.

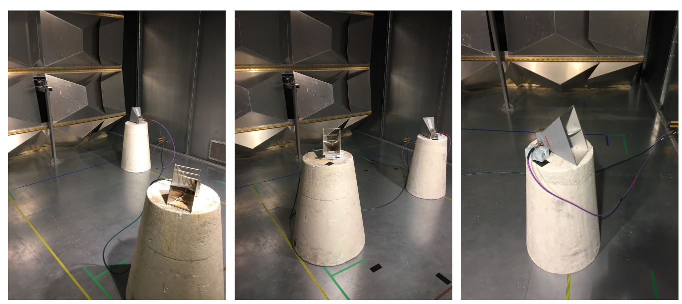

(a) (b) (c)

Fig. 3. Photographs of the three situations in the RC; between B and C, only the orientation of antenna II is changed.

Case C, 1.6 m is estimated in Table I while the first peak in Fig. 5 is observed at 1.3 m. This deviation is most likely due to errors in the measurement of antenna positioning, especially its rotation in the azimuth plane. Cases A and B involve the stirrer, and will be studied in more detail in Section IV.

Taking into account the possibility of measurement errors of the antenna positioning (especially rotation), the non-infinitesimal beamwidth of the antennas and the possibility of a shifting phase center, the estimated transition distance from very-early-time to early-time is taken as 1 m for both reflection parameters. Note that, strictly speaking, the duration of very-early-time differs per antenna positioning, and could be extended further into time for e.g. S_{11} of Case A.

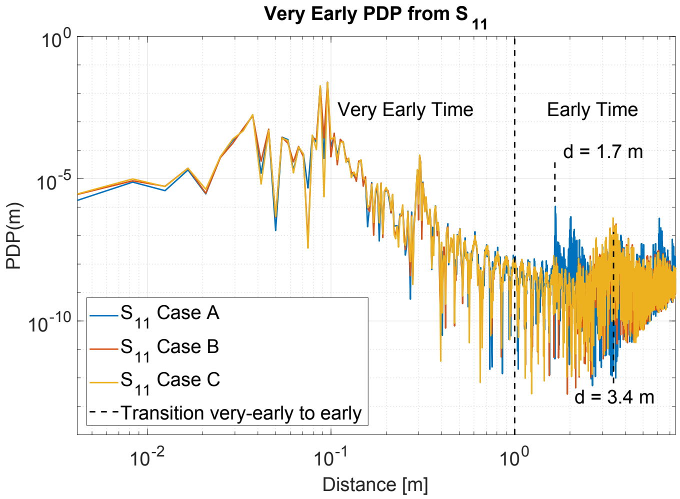

Fig. 4. Very-early-time PDP as a function of distance traveled obtained from S_{11} (antenna I) measurements.

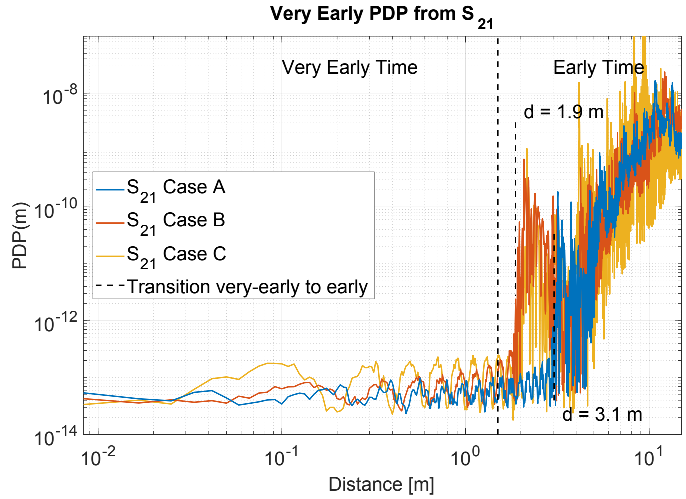

Fig. 6. Very-early-time PDP as a function of distance traveled obtained from S_{21} measurements.

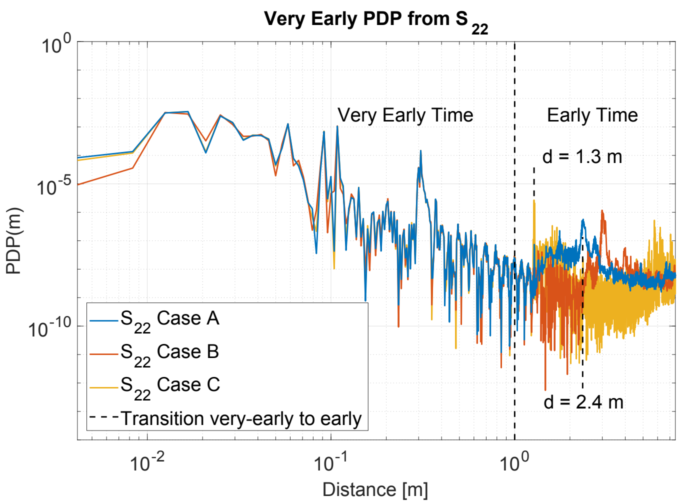

Fig. 5. Very-early-time PDP as a function of distance traveled obtained from S_{22} (antenna II) measurements.

The very-early-time behavior of S_{21} is shown in Fig. 6 for all three cases. It can be observed that the signal is at noise floor during the entire period of the very-early-time. The approximate distance between the antennas largely accounts for the time it takes for the signal to rise above noise floor: reading from the figure approximately 3.1 m for case A and 1.9 m for Cases B and C, compared to 2.4 m distance in case A and 1.6 m distance in Cases B and C as indicated in Table I. Note that in all cases the distance obtained in the PDP measurements is higher, probably due to the low back-radiation of the horn antennas which were not directed at one another.

IV. Early-Time

When the very-early-time ends, the early-time starts. Like the very-early-time behavior the early-time behavior is best shown on a logarithmic scale, but with a different range. The early-time behavior has some interesting properties, which will be discussed in this Section.

Fig. 7, 8 and 9 zoom in to the early-time behavior observed at the end of the intervals shown in Fig. 4, 5 and 6, respectively. This allows for a much clearer view of the early-time behavior. It can be observed from Fig. 7 and 8 that the behavior is mostly different when comparing the measurements. This is due to the different direct environment that is encountered at each of the positions. Case B and Case C match in the results for S_{11} for this period, since antenna I was not moved between Case B and Case C. The same peaks as discussed in Section III (1.7 m for Case A and 3.4 m for Case B and Case C) can be observed in S_{11}, as well as another clearly distinguishable peak for Case A at 2.0 m, since in that case antenna I was pointing close to a corner.

For S_{22} the sharp peak for Case C discussed in Section III can now be observed more clearly. In addition, two curves show behavior that is clearly distinct from the other curves: Case A and Case B of S_{22}. These are the cases where the antenna is pointed directly at the stirrer (Fig. 2). Since the stirrer is moved, this results in a different first-reflection distance for each of the samples before averaging. In turn, after averaging, this results in a broad bump. Due to the stirrer shaping this bump can have several peaks, as a different part of the stirrer shape starts acting as a point of first reflection. The bumps are centered in the PDP around 2.4 m and 3.0 m for Case B and Case C, respectively, corresponding to approximate distance to stirrer center positions of 2.1 m and 3.4 m (adding half the stirrer travel to R_{II}). Considering the shaping of the stirrer and measurement uncertainty of antenna positioning, these numbers are according to expectation.

In the transmission parameter, shown in Fig. 9, the direct coupling between the antennas is observed at the earliest point in time, as discussed previously in Section III. After that point in time, some distinct peaks can be observed, each indicating a path through which the antennas couple

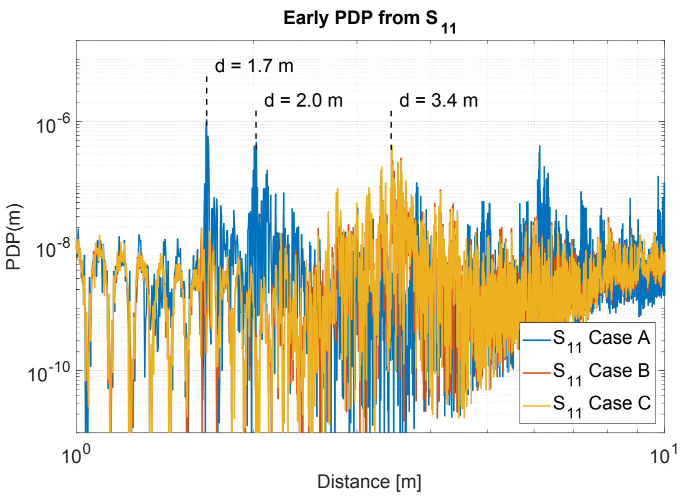

Fig. 7. Early-time PDP as a function of distance traveled obtained from S_{11} (antenna I) measurements.

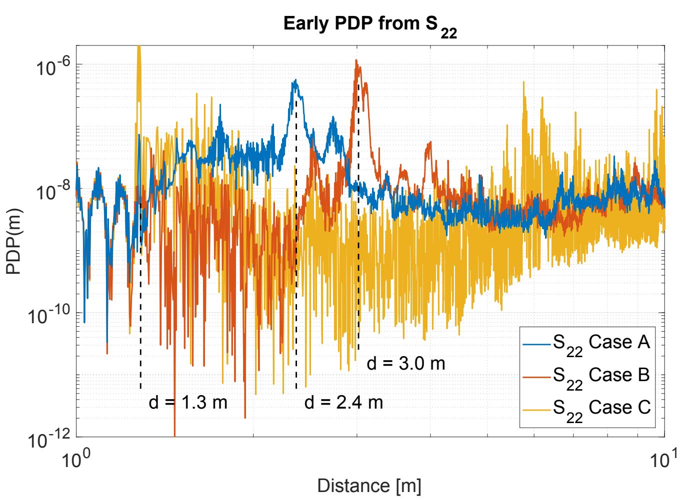

Fig. 8. Early-time PDP as a function of distance traveled obtained from S_{22} (antenna II) measurements.

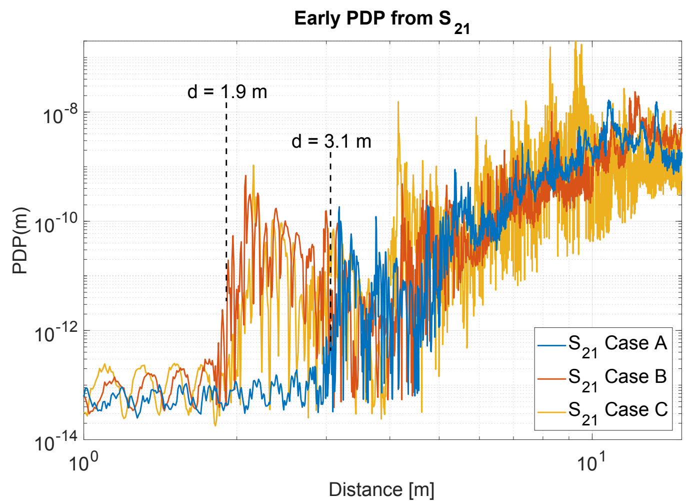

Fig. 9. Early-time PDP as a function of distance traveled obtained from S_{21} measurements.

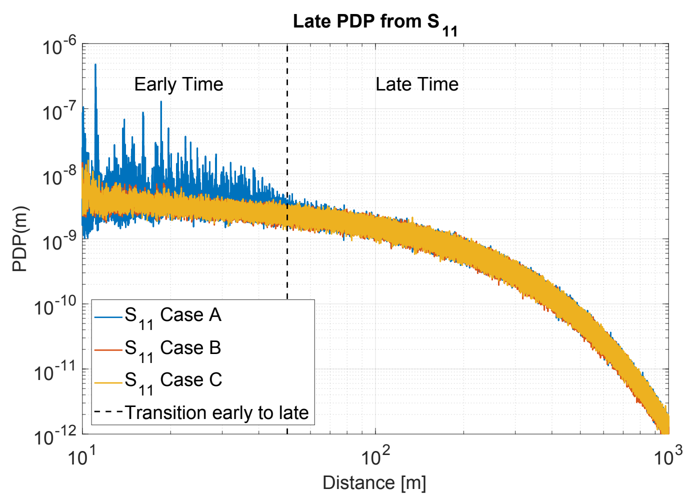

Fig. 10. Late-time PDP as a function of distance traveled obtained from S_{11} (antenna I) measurements.

significantly. However, as all these paths include multiple reflections, it is hard to say which path each peak originates from.

The early-time behavior ends when the chamber-buildup is finished, and the signals converge to their desired stochastic behavior. This transition is studied in the next Section.

V. Late-Time

Finally, after the very-early-time and early-time periods, the wave travels into the period known as the late-time [3]. In an ideal chamber the deterministic behavior has completely disappeared in this period, providing a fully stochastic environment. The late time is by far the longest period in the RC, ranging from the end of the early-time to that point in time at which the signal drops below the VNA's dynamic range (which will take longer in a high-Q RC since the losses are lower). Due to this relatively long duration, it is usually most convenient to observe the late-time behavior on a semilogarithmic scale. However, since for this paper the earliest part of the late behavior is most interesting, it is shown on a logarithmic scale like the earlier results.

In Fig. 10, 11 and 12 the results for the late-time behavior are shown for S_{11}, S_{22} and S_{21}, respectively. In Case A the signal converge towards the exponential decay [1], [3], [9], [10], [12] after approximately 50 m of total distance traveled. In cases B and C this happens significantly earlier: after approximately 25 m. For the present room, the mean-free path [13] is approximately $l_c = 2.7$ m, so 25 m corresponds to approximately $9l_c$ while 50 m corresponds to approximately $18l_c$. Earlier, it was proposed that reverberation occurs after $8l_c$ to $10l_c$ [13]. Here, Case A is the 'odd one' in that it converges later than the other two cases and earlier proposals. Therefore it can be seen that the time it takes to reach this condition depends on antenna positioning within this RC. The frequency-domain analogue of this would be a larger unstirred contribution, resulting in less remaining dynamic range for the

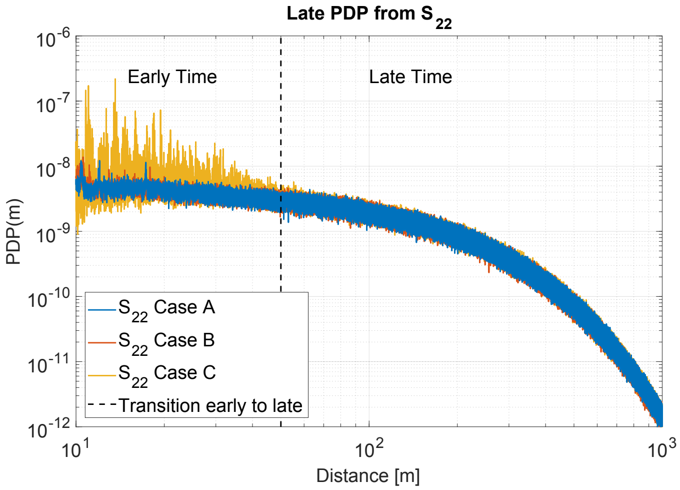

Fig. 11. Late-time PDP as a function of distance traveled obtained from S_{22} (antenna II) measurements.

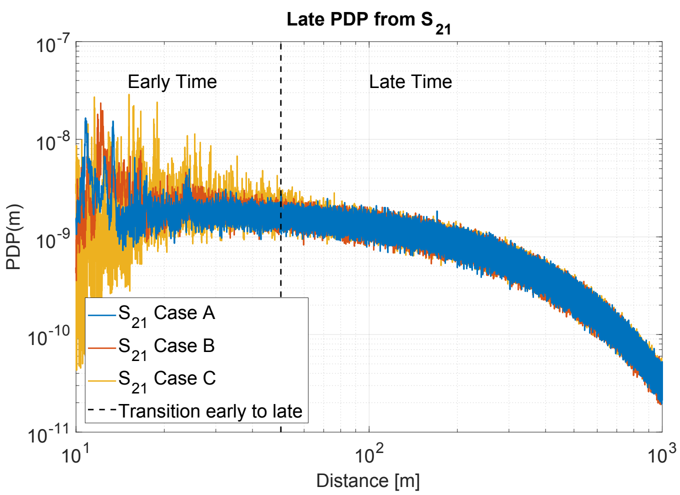

Fig. 12. Late-time PDP as a function of distance traveled obtained from S_{21} measurements.

stirred contributions.

VI. Conclusion

In this paper the ensemble-average wave is followed starting from its creation at the antenna reference plane, leading to the novel observation of three regimes: very-early-time, early-time and late-time. In the very-early-time the response is dictated by the antenna's behavior, the duration of which is dependent on antenna positioning and, mainly, the distance from its radiating aperture to a reflecting surface at boresight. In the early-time period the wave starts interacting with the environment. A very interesting effect is that, due to the taking of the ensemble average, the linear stirrer movement can be observed as clearly distinct bumps in the PDP during early-time behavior. In the late period the expected exponential decay is observed, and it is shown that the transition point from early to late behavior is dependent on antenna placement in the room that was used. After chasing the wave traveling at lightspeed for a kilometer, it is finally caught when the chamber losses cause the PDP to decay into noise floor.

References

[1] E. Genender, C. L. Holloway, K. A. Remley, J. M. Ladbury, G. Koepke, and H. Garbe, "Simulating the Multipath Channel With a Reverberation Chamber: Application to Bit Error Rate Measurements," *IEEE Trans. Electromagn. Compat.*, vol. 52, no. 4, pp. 766–777, nov 2010.

[2] P. S. Kildal, A. Hussain, X. Chen, C. Orlenius, A. Skårbratt, J. Åsberg, T. Svensson, and T. Eriksson, "Threshold receiver model for throughput of wireless devices with mimo and frequency diversity measured in reverberation chamber," *IEEE Antennas Wirel. Propag. Lett.*, vol. 10, pp. 1201–1204, 2011.

[3] C. L. Holloway, H. A. Shah, R. J. Pirkl, K. A. Remley, D. A. Hill, and J. Ladbury, "Early Time Behavior in Reverberation Chambers and Its Effect on the Relationships Between Coherence Bandwidth, Chamber Decay Time, RMS Delay Spread, and the Chamber Buildup Time," *IEEE Trans. Electromagn. Compat.*, vol. 54, no. 4, pp. 714–725, aug 2012.

[4] B. P.-s. Kildal, C. Orlenius, and J. Carlsson, "OTA Testing in Multipath of Antennas and Wireless Devices With MIMO and OFDM Use of a reverberation chamber for testing wireless devices in rich isotropic," *Ieee*, vol. 100, no. 7, 2012.

[5] W. T. C. Burger, C. L. Holloway, and K. A. Remley, "Proximity and orientation influence on Q-factor with respect to large-form-factor loads in a reverberation chamber," pp. 369–374, 2013.

[6] X. Chen, "Throughput modeling and measurement in an isotropic-scattering reverberation chamber," *IEEE Trans. Antennas Propag.*, vol. 62, no. 4, pp. 2130–2139, 2014.

[7] A. Hussain, P. S. Kildal, and A. A. Glazunov, "Interpreting the total isotropic sensitivity and diversity gain of LTE-enabled wireless devices from over-the-air throughput measurements in reverberation chambers," *IEEE Access*, vol. 3, pp. 131–145, 2015.

[8] R. Measel, C. S. Lester, D. J. Bucci, K. Wanuga, G. Tait, R. Primerano, K. R. Dandekar, and M. Kam, "An Empirical Study on the Performance of Wireless OFDM Communications in Highly Reverberant Environments," *IEEE Trans. Wirel. Commun.*, vol. 15, no. 7, pp. 4802–4812, 2016.

[9] C. L. Holloway, H. A. Shah, R. J. Pirkl, W. F. Young, D. A. Hill, and J. Ladbury, "Reverberation Chamber Techniques for Determining the Radiation and Total Efficiency of Antennas," *IEEE Trans. Antennas Propag.*, vol. 60, no. 4, pp. 1758–1770, apr 2012.

[10] X. Zhang, M. Robinson, and I. Flintoft, "On measurement of reverberation chamber time constant and related curve fitting techniques," in *2015 IEEE Int. Symp. Electromagn. Compat.*, no. 1. IEEE, aug 2015, pp. 406–411.

[11] R. Serra, A. C. Marvin, F. Moglie, V. M. Primiani, A. Cozza, L. R. Arnaut, Y. Huang, M. O. Hatfield, M. Klingler, and F. Leferink, "Reverberation chambers a la carte: An overview of the different mode-stirring techniques," *IEEE Electromagn. Compat. Mag.*, vol. 6, no. 1, pp. 63–78, 2017.

[12] D. A. Hill, *Electromagnetic Fields in Cavities*. Hoboken, NJ, USA: John Wiley & Sons, Inc., sep 2009, vol. 43, no. 08.

[13] C. Holloway, M. Cotton, and P. McKenna, "A model for predicting the power delay profile characteristics inside a room," *IEEE Trans. Veh. Technol.*, vol. 48, no. 4, pp. 1110–1120, jul 1999.